

Full Length Article

Preparation and photo Fenton-like activities of high crystalline CuO fibers

Yan Zhang, Jing He, Ruixia Shi*, Ping Yang*

School of Material Science and Engineering, University of Jinan, 250022 Jinan, PR China

ARTICLE INFO

Article history:

Received 30 December 2016

Received in revised form 1 June 2017

Accepted 4 June 2017

Available online 8 June 2017

Keywords:

CuO

Electrospinning

Photo-Fenton

Full spectrum

H₂O₂

ABSTRACT

CuO fibers were successfully fabricated by a simple electrospinning method, followed by calcination. Some experimental parameters such as the content of Cu(NO₃)₂·3H₂O, the content of PVP, the stirring time, the applied voltage, as well the calcination temperature were investigated, respectively, and their influences on the morphologies of fibers and the spinnability of precursor solution were analyzed. The CuO fibers calcined at 550 °C consisted of numerous CuO grains exhibited a well-crystalline structure. Furthermore, the CuO fibers demonstrated effective photo-Fenton degradation to methyl orange with the assist of H₂O₂ and the adding volume of H₂O₂ affects the degradation activities greatly. The degradation rate of methyl orange by the CuO fibers in the presence of 238.8 mmol/L H₂O₂ is 3.8 times as much as one by P25 alone under the irradiation of Xe lamp. The degradation ratio of methyl orange could achieve 83% in 180 min. The enhanced photocatalytic activities of the CuO fibers were attributed to two aspects: one is the well-crystalline of CuO fibers; the other is that H₂O₂ accepted the photogenerated electrons and holes effectively, which not only prevented the recombination of charge carriers but also produced additional •OH. In this work, the formation and photocatalysis mechanisms of CuO fibers were also investigated.

© 2017 Elsevier B.V. All rights reserved.

1. Introduction

Copper oxide (CuO), a p-type semiconductor with a narrow band gap of 1.7 eV, has attracted great interests owing to its outstanding optical, magnetic and electric properties, and has been applied in diverse fields [1] such as photocatalysis [2], gas sensors [3,4], optical switch, metallurgy reagent [5], high-critical-temperature superconductors, lithium batteries [6] and solar cells [7]. Among these fields, photocatalysis has recently taken much attention with the aggravation of environmental pollution [8]. However, CuO was always studied to combine with other compounds to degrade pollutions in wastewater, such as CuO/ZnO [9,10], CuO/TiO₂ [11], CuO/SnO₂ [12], CuO/BiVO₄ [13], CuO/grapheme [14] and CuO/clinoptilolite [15] in the past. Researches about using CuO alone as the photocatalyst were rarely reported for its inability to produce abundant •OH radicals [16]. Since the last few years, CuO, as the single-component photocatalyst, has received much attention to deal with the water pollution [17]. Meshram et al. [18] have synthesized CuO nanostructures having different morpholo-

gies such as spherical, vesicular, nanosheet and platelet and tested their photocatalytic properties. Behrouz et al. [19] have prepared flower-like CuO nanostructures and aggregated CuO nanoparticles in the form of clusters and investigated their catalytic activities. Results show that the samples have a good degradation effect for Rhodamine B (RhB) under UV-light irradiation. Unfortunately, there are few reports for the research about one dimensional (1D) structure of CuO and its photocatalysis. 1D structural materials have many potential scientific and technological applications [20] for their high surface-to-volume ratio, enhanced charge carrier mobility and small pore size [21].

Nowadays, there are various methods [22] such as template method [23], sol-gel technique, hydrothermal method and electrospinning [24] to produce 1D structural materials. Compared with other methods, electrospinning is considered as a simple, versatile and effective technique to prepare fibers with high surface to volume ratio [25] and this method has gained high international recognition. In addition, electrospinning method is very flexible in controlling the diameter and microstructure of fibers [26] by adjusting the experimental parameters. Thus, electrospinning has been widely applied to prepare polymers [27], ceramics [28] and composite fibers [29,30]. A large number of papers reported that

* Corresponding authors.

E-mail addresses: mse-shirx@ujn.edu.cn (R. Shi), yangp@ujn.edu.cn (P. Yang).

the electrospinning-synthesized fibers possess good photocatalytic properties [31,32].

Upon the irradiation, CuO, a narrow gap semiconductor, has broader adsorption range [33], which enhanced the generating density of charge carriers and was benefit to elevate its photocatalytic activity. But the rapid combination of electrons and holes is a major limiting factor for the degradation of pollutions. Hence, preventing the combination of charge carriers and improving their utilization have become a significant way for increasing the photocatalytic activity of CuO. Therefore, many methods have been applied to enhance the degradation efficiency. Among them, the addition of H_2O_2 in the reaction system has been proven to be an effective method [34,35]. Catalysts containing iron is famous for the photo-Fenton reaction when adding H_2O_2 . Copper also can improve the degradation efficiency via the Fenton-like reactions [36,37].

In this work, we prepared pure well-crystalline CuO fibers by a facile electrospinning method, combined with subsequent calcination. A series of experimental parameters were investigated systematically. The possible formation mechanism of CuO fibers was proposed. Furthermore, H_2O_2 -assisted photo Fenton-like process was carried out. And the result indicated that the as-prepared CuO fibers exhibited high photo Fenton-like activities for the degradation of MO in the presence of H_2O_2 . The photocatalysis mechanism was also discussed.

2. Experimental section

2.1. Materials

Copper (II) nitrate hydrate ($\text{Cu}(\text{NO}_3)_2 \cdot 3\text{H}_2\text{O}$) was supplied by Sinopharm Chemical Reagent Co. Ltd. Polyvinylpyrrolidone (PVP, $M_w = 1,300,000$) was obtained from Aladdin Industrial Corporation. The Methyl Orange (MO) was purchased from Tianjin Guangcheng Chemical Reagent Co. Ltd. H_2O_2 (30%, w/w) was obtained by Laiyang Kangde Reagent Co. Ltd. Anhydrous ethanol was supplied by Tianjin Fuyu Chemical Industry Co. Ltd. Deionized water was produced from Millipore Synergy ultrapure water system. P25 was purchased from Beijing Shangwei Kelin Co. Ltd. All of the commercial materials were of analytical grade and used without further purification.

2.2. Preparation of $\text{Cu}(\text{NO}_3)_2/\text{PVP}$ composite nanofibers and CuO nanofibers

In a typical procedure, $\text{Cu}(\text{NO}_3)_2/\text{PVP}$ composite nanofibers were prepared as follows: firstly, $\text{Cu}(\text{NO}_3)_2 \cdot 3\text{H}_2\text{O}$ was dissolved in the mixed solvents of 2 mL deionized water and 10 mL anhydrous ethanol. Subsequently, a certain quantity of PVP was added into the solution under the constant stirring. After stirring for several hours at room temperature, the precursor solution was drawn into a 5 mL syringe for electrospinning at room temperature in air. The injection flow rate and the nozzle-collector distance were 0.9 mL/h and 18 cm, respectively. The as-spun fibers were dried at 60°C for several hours. Finally, the fibers were calcined in air at an appropriate temperature for 2 h with a heat rate of $2^\circ\text{C}/\text{min}$ to obtain pure CuO fibers.

To investigate the effects of different factors on the morphology of CuO/PVP composite fibers, a series of parameters were adjusted. Detailed preparation conditions were presented in Table 1.

2.3. Characterization

The X-ray diffraction of the resulting samples was characterized by X-ray diffractometer (XRD, D8-ADVANCE of Bruker Corporation) with a Cu K α target. The morphology of the samples was investigated by field-emission scanning electron microscopy

(FESEM, QUANTA-250FEG). Thermal behaviors for the composite fibers were studied by thermal gravimetric analysis (TGA, TGA/DCSC1/1600HT of Mettler Corporation) under argon atmosphere with a heating rate of $10^\circ\text{C}/\text{min}$. Photoluminescence (PL) emission spectrum was recorded in F-4600 Hitachi fluorescence spectrometer. The adsorption capacity of MO solution was studied by a UV-vis spectrophotometer (U-4100 of Hitachi Corporation) with a quartz cell.

2.4. Photocatalytic activity

The visible-light photocatalytic activity of CuO fibers were demonstrated by monitoring photocatalytic degradation of MO dye in aqueous solutions. An 18 W Xe lamp was positioned atop the reaction vessel as the source. In a typical experiment, 10 mg catalyst was dispersed into 20 mL MO solution (2.5 mg/L) for photocatalytic examination under constant magnetic stirring and then the solution was kept for 60 min in the dark to achieve the adsorption-desorption equilibrium of MO on the catalysts. After that, a certain amount of H_2O_2 (30%, w/w) was added into the solution and the solution was exposed to visible-light irradiation. At 30 min intervals, 2 mL of suspension was taken out and centrifuged immediately. The degradation of MO was monitored by measuring absorbance at $\lambda_{\text{max}} = 462 \text{ nm}$ with a UV-vis spectrophotometer. The copper leaching was determined by inductively coupled plasma optical emission spectrometry (ICP-OES) (IRIS Intrepid II XSP, Thermo Elemental, USA).

3. Results and discussion

3.1. Fabrication and characterization of $\text{Cu}(\text{NO}_3)_2/\text{PVP}$ composite fibers

The $\text{Cu}(\text{NO}_3)_2/\text{PVP}$ composite fibers were fabricated by electrospinning method. To obtain uniform and smooth composite fibers, batch experiments were carried out.

3.1.1. The effects of the content of PVP

The content of PVP is one of the most important parameters. In this experiment, the content of PVP (measured by the mass fraction of PVP, $\omega_{\text{PVP}} = \frac{m_{\text{PVP}}}{m_{\text{H}_2\text{O}} + m_{\text{C}_2\text{H}_6\text{O}} + m_{\text{Cu}(\text{NO}_3)_2 \cdot 3\text{H}_2\text{O}} + m_{\text{PVP}}} \times 100\%$) was adjusted gradually from 5.3 wt% (sample 1) to 4.5 wt% (sample 3), as shown in Table 1, to investigate its effect on the spinning process. For sample 1, it was observed that the nozzle was blocked during the spinning process, prohibiting the formation of fibers seriously. By decreasing the content of PVP, those phenomena were relieved and the spinning rate was increased effectively. Electrospinning process ran smoothly and no blocking was observed when the content of PVP was reduced to 4.9 wt% (sample 2). For sample 3, however, some droplets dripped from the nozzle to the fibers, causing the as-spun fibers were dissolved. Hence, 4.9 wt% PVP (sample 2) was suitable for this experiment. PVP, as spinning additive, is crucial for the spinnability of spinning solution, and its content is proportional to viscosity. When the viscosity is very high spinning solution shows poor spinnability because the electrostatic force is less than the sum of surface tension and viscous force. With the decreasing of viscosity, the viscous force would decrease and the electrostatic force is greater than the sum of surface tension and viscous force, which leads to the formation of Taylor cone at the nozzle. Otherwise, the solution with low viscosity would not be stretched to form fibers.

3.1.2. Effects of the content of $\text{Cu}(\text{NO}_3)_2 \cdot 3\text{H}_2\text{O}$

To explore the effects of metallic salt content on this experimental system, the content was increased to 0.35 g (sample 4)

Table 1

Preparation conditions of spinning solutions.

Samples	Cu(NO ₃) ₂ ·3H ₂ O (g)	PVP (wt%)	The applied voltage (kV)	Stirring time (h)
1	0.30	5.3	13	2
2	0.30	4.9	13	2
3	0.30	4.5	13	2
4	0.35	4.9	13	2
5	0.40	4.9	13	2
6	0.45	4.9	13	2
7	0.35	4.9	13	1
8	0.35	4.9	13	4
9	0.35	4.9	12	4
10	0.35	4.9	11	4

Fig. 1. SEM images of Cu(NO₃)₂/PVP composite fibers of (a) sample 2 and (b) sample 4.**Fig. 2.** SEM images of Cu(NO₃)₂/PVP composite fibers of (a) sample 4 and (b) sample 8.

from 0.30 g (sample 2). Results show that the electrospinning process ran smoothly. However some fibers floated over the collector during the spinning process when the content was increased to 0.40 g (sample 5). And this phenomenon got worse when the Cu(NO₃)₂·3H₂O content was further increased to 0.45 g (sample 6). The main reason is that fibers with higher salt content would be acted upon by a larger electrostatic force in the electrical fields and the enhanced force made fibers overcome their own gravity and float in the air. Judging by the electrospinning phenomena, the SEM images of the sample 2 and 4 are shown in Fig. 1. Compared with sample 4, not only the fiber surface of sample 2 became rougher but the phenomenon of adhesion was being aggravated. Thus, the proper content of Cu(NO₃)₂·3H₂O is 0.35 g in this experiment.

3.1.3. Effects of the stirring time

Based on the above experimental results, the stirring time was adjusted. The solution stirred for 1 h (sample 7) was spun and it is observed that small amount of droplets produced at irregular intervals during the spinning process. But no droplets appeared when the precursor solution was stirred for 2 (sample 4) or 4 h (sample

8). This phenomenon is chiefly ascribed to the homogeneity of the solution. In order to further ascertain an applicable stirring time, the microstructures of sample 4 and 8 were investigated by SEM and their high magnification images were shown in Fig. 2. The surfaces of sample 8 are very smooth, while that of sample 4 are uneven and rough. As known to us, the longer time the solution is stirred, the more uniform solution was obtained. Based on the SEM images, the stirring time of 4 h was enough to gain uniform and smooth composite fibers.

3.1.4. Effects of the applied voltage

The applied voltage is an important electrospinning parameter, which determines the intensity of electrostatic field, thus affecting the microstructure of the as-prepared fibers. Adjusting the applied voltage from 13 kV (sample 8) to 12 kV (sample 9) and 11 kV (sample 10) gradually, different experimental phenomena were barely observed during the spinning process of these three samples. To investigate the effects of the applied voltage on the microstructure of fibers, the SEM images of sample 8 and 10 are shown in Fig. 3. It is very clear that the fibers of sample 10 were arranged

Fig. 3. SEM images of $\text{Cu}(\text{NO}_3)_2/\text{PVP}$ composite fibers of (a) sample 8 and (b) sample 10.

Fig. 4. TGA curve of $\text{Cu}(\text{NO}_3)_2/\text{PVP}$ composite fibers.

in a direction, but fibers of sample 8 are in random orientation. And the diameters of sample 8 were smaller than ones of sample 10. The electrostatic force increased with the raising applied voltage, causing the jets were stretched adequately and the average diameter of fibers reduced. Additionally, the fibers were apt to disperse towards every direction due to the enhanced repulsive forces between fibers. Judging by the microstructures of two samples, 13 kV applied voltage is suitable in this work.

3.1.5. TGA of $\text{Cu}(\text{NO}_3)_2/\text{PVP}$ composite fibers

Fig. 4 shows the thermal analysis curves of the $\text{Cu}(\text{NO}_3)_2/\text{PVP}$ composite fibers of sample 8 under argon atmosphere. Obviously, the weight loss can be divided into three major parts. Firstly, in the temperature range of 50–150 °C, a nearly 15% weight loss occurred for the volatilization of deionized water and ethanol. Secondly, a remarkable weight loss of approximate 35% can be observed from 220 °C to 240 °C, which is attributed to the decomposition of $\text{Cu}(\text{NO}_3)_2 \cdot 3\text{H}_2\text{O}$. Finally, the decomposition of PVP caused a weight loss about 20% at 320–470 °C. After 500 °C, the weight of fibers basically reached a constant level, indicating that most of the volatiles, NO_3^- groups of nitrates and organics had been removed. Hence, 500 °C was selected as the initial calcination temperature.

3.2. CuO fibers

3.2.1. Fabrication and characterization of CuO fibers

Fig. 5a depicts the microstructure of the fibers of sample 8 calcined at 500 °C. As is evident, the calcined fibers were rough and composed of numerous grains. The average diameter is about 1 μm . Observing the surface of the fibers, it is obvious that growth of the crystalline grain is incomplete and the grain boundaries are unclear, suggesting that PVP was not decomposed completely. Thus, 600 °C

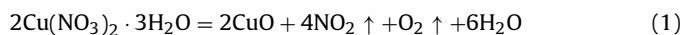
was applied to calcine the composite fibers and the SEM image of the as-prepared fibers is shown in Fig. 5b. Results show that the crystallinity of grains became better and the grain size enlarged but the CuO fibers were observed to be broken seriously, which should be attributed to the excessive growth of CuO grains caused by the higher calcination temperature. To adjust the morphology of the CuO fibers, the composite fibers were calcined at 550 °C (Fig. 5c). It is clearly that the fibers are continuous, meanwhile, the well-crystalline CuO grains possess more uniform size. In general, 550 °C is a proper calcination temperature in the experiment.

In order to evaluate the crystal structure of the as-prepared fibers, sample 8 calcined at 550 °C was investigated by XRD and the pattern was shown in Fig. 6. The characteristic diffraction peaks at 32.5°, 35.5°, 38.7°, 48.7°, 53.5°, 58.3°, 61.5°, 65.8°, 68.1°, 72.4°, 75.0° can be indexed to the (110), (11 $\bar{1}$), (111), (20 $\bar{2}$), (020), (022), (11 $\bar{3}$), (022), (220), (311) and (004) reflections, respectively, which are in agreement with the monoclinic structured CuO (JCPDS No.48-1548) with lattice constant of $a = 0.469 \text{ nm}$, $b = 0.342 \text{ nm}$ and $c = 0.513 \text{ nm}$. Furthermore, the sharp peaks and no peaks of impurities indicate that pure well-crystalline CuO fibers can be obtained via the calcination of 550 °C.

3.2.2. Formation mechanism of CuO fibers

On the basis of the aforementioned observations and analysis, a possible formation mechanism of CuO fibers is proposed as follows.

A possible formation process of CuO fibers is demonstrated in Fig. 7. At first, the $\text{Cu}(\text{NO}_3)_2/\text{PVP}$ composite fibers (Fig. 7a) were obtained through electrospinning. And then the solvents evaporated at low calcination temperature. When the temperature was increased to 130 °C, PVP started to melt, which caused the adhesion of adjacent fibers. With the further increase of temperature, $\text{Cu}(\text{NO}_3)_2 \cdot 3\text{H}_2\text{O}$ decomposed (Eqs. (1)) and CuO crystal nucleus were formed on the fibers surface. Meanwhile, the long-chain molecules of PVP prevent the aggregation of CuO crystal nucleus and the destruction of the fiber-structure effectively.



Subsequently, PVP started to decompose gradually (Eqs. (2)) and CuO crystal nucleus began to grow. During the process of crystal growth, the driving force from the difference of Gibbs free energy between both sides of grain boundary leads to the moving of grain boundary. To reduce the grain boundary area and the grain boundary energy, part of grains disappeared or decreased in size due to the growth. In the end of the stage, average grain size increased.

Fig. 5. SEM images of CuO fibers of sample 8 calcined at different temperature: (a) 500 °C, (b) 600 °C, (c) 550 °C.

Fig. 6. XRD pattern of CuO fibers calcined at 550 °C.

Finally, with the complete elimination of PVP, the CuO crystal grains connected to each other and formed the CuO fibers.

(2)

3.3. Photocatalytic properties and analysis

3.3.1. Photocatalytic properties

MO was chosen as the model pollutant to demonstrate the photocatalytic properties of CuO fibers in the presence of H₂O₂. Fig. 8a–e shows the UV–vis absorption spectrum of MO in different

photocatalytic experimental conditions. As a matter of convenience, the added H₂O₂ and catalysts is labeled as $x\text{H}_2\text{O}_2\text{-}y\text{CuO}$, where x is the volume (mL) of H₂O₂ and y is the weight (mg) of CuO. It can be found that the absorption peak declined remarkably when H₂O₂ existed (Fig. 8b–d), while only a slight decrease was observed if the catalytic system without any H₂O₂ (Fig. 8a), which demonstrate H₂O₂ plays a very important role in the catalytic process. Additionally, the adding volume of H₂O₂ has a significant impact on the catalytic effect. Compared with Fig. 8a, it is quite clear that the photodegradation rate of MO elevated dramatically when 0.2 mL H₂O₂ (the concentration of H₂O₂ in the photocatalytic system is 96.9 mmol/L) was added (Fig. 8b) and that was further enhanced when 0.5 mL ($C_{\text{H}_2\text{O}_2} = 238.8 \text{ mmol/L}$) or 1.0 mL H₂O₂ ($C_{\text{H}_2\text{O}_2} = 466.2 \text{ mmol/L}$) was added, respectively. Moreover, an experiment in the absence of CuO fibers (Fig. 8e) was carried out for investigating the role of CuO fibers during the degradation of MO. Results show that the absorption peak did not decline, conversely, increase in a small range with the time, as the result of the unobvious decomposition of MO and the evaporation of water under continuous irradiation. So the decomposition of MO was almost unaffected by H₂O₂ alone. Favorable photodegradation of MO only come true in the presence of H₂O₂ and CuO fibers at the same time. Fig. 8f shows the concentration degradation profiles of MO versus time. Obviously, the degradation rate increased with increasing in the adding volume of H₂O₂ (to 0.5 mL) and then remained unchanged basically. The MO degradation ratio catalyzed by CuO fibers alone at 180 min was just about 10%, while it was sharply increased to 83% when 0.5 mL H₂O₂ was added and the ratio catalyzed by 1.0H₂O₂-10CuO was basically similar to 0.5H₂O₂-10CuO. This indicates that the as-prepared CuO fibers have better photocatalytic activities in the presence of H₂O₂.

In order to evaluate the MO degradation effects of CuO fibers, the photocatalytic activities of P25 without adding H₂O₂ were measured under the full spectrum irradiation (Fig. 8f). It is evident that P25 displayed relatively low photoactivity, resulting in decreases of

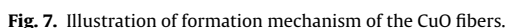


Fig. 7. Illustration of formation mechanism of the CuO fibers.

22% in the concentration of MO during 180 min. So the MO degradation rate by the CuO fibers is 3.8 times as much as one by P25 alone.

The room temperature photoluminescence spectrum of CuO fibers was presented in Fig. 9, at the excitation of 325 nm. The spectrum shows six sharp emission peaks (371, 388, 456, 472, 532 and 554 nm) and a broad emission peak centered at 750–800 nm. The peaks at 371 and 388 nm are ascribed to the UV emission of near band-edge (NBE) causing by the recombination of electron-hole pair in free excitons [38,39]. The peaks in the blue region at 456 and 473 nm are caused by transition vacancy of oxygen and interstitial oxygen [40,41]. The emission peaks at 532 and 554 nm, which correspond to green emission, arise from the singly ionized oxygen vacancy of CuO fibers [42,43]. Furthermore, the broad emission peak at 750–800 nm (IR band) was attributed to the specific surface effect, which results in the red-shift of the fluorescence emission [44]. The high PL intensities at 371 and 388 nm reflect a low separation rate of photo-induced carriers, which confirm the bad photocatalysis activities of CuO fibers alone and H₂O₂ play a very significant role as electron acceptor in the catalysis process.

To clarify the main active species in the MO degradation process photocatalyzed by CuO fibers, trapping experiments in the presence of 0.5 mL H₂O₂ ($C_{H_2O_2} = 238.8$ mmol/L) and 10 mg CuO were carried out. As shown in Fig. 10, 0.2 mmol AgNO₃ (e⁻ quencher), 0.2 mmol KI (h⁺ scavenger) and 2 mL isopropanol (IPA, •OH quencher) were added, respectively. The degradation of MO was greatly influenced by the addition of the three scavengers, indicating e⁻, h⁺ and •OH were the active species in the reaction. The degradation rate sharply decreased from 83% to 17%, 5% and 15% since the AgNO₃, KI and IPA were separately introduced into the photocatalytic system.

3.3.2. Photocatalysis mechanism

As is well-known, two major factors affect the photocatalysis activities: the light absorption capability of photocatalyst and separation of excited electron-hole pairs [45]. According to the above experiments and analysis, a possible photocatalysis mechanism of

MO when the CuO fibers and H₂O₂ was employed is shown in Fig. 11. In the system without H₂O₂ (Fig. 11a), the CuO was excited and produced photon-generated carriers (Eq. (3)) under the light radiation. The holes could react with H₂O to generate hydroxyl radical (•OH) (Eqs. (4)) or directly oxidize MO (Eqs. (5)). However, the electrons accumulated in the E_{CB} of CuO have no enough reduction ability to reduce O₂ to form •O₂⁻ ($E^0(O_2/\bullet O_2^-) = -0.046$ eV vs. NHE) [46,47]. With $E^0 = +3.06$ V, •OH is a kind of strong oxidant [48,49] and could oxidize the MO to inorganic small molecular compounds (Eqs. (6)). Therefore, only •OH could oxidize the MO in the photocatalytic mechanism of CuO. For no e⁻ acceptor in this system, e⁻ species accumulated in the conduction band were prone to dropping and recombining with h⁺, which leads to the low photocatalysis activities thus the MO was degraded by the CuO fibers only 10% (Fig. 8a).

When H₂O₂ was added in the process (Fig. 11b), the MO removal is mainly attributed to heterogeneous photo Fenton-like reactions. On the one side, H₂O₂ could accept the electrons and holes to produce active •OH species (Eqs. (7)) and •O₂⁻ species [50] (Eqs. (8)), respectively. And the •O₂⁻ species are further reacted with H₂O₂ to generate •OH (Eqs. (9)). Then, the •OH radicals oxidize the MO to inorganic small molecular compounds. For another, the results show that the copper leaching is 1.44 mg/L after the photocatalysis reaction, which indicated that copper were involved into the reaction [51]. Firstly, the reactions were initiated by the photo-reduction of Cu²⁺ on the surface of CuO fibers to Cu⁺ under irradiation. Secondly, H₂O₂ reacted with Cu⁺ to form •OH and Cu²⁺, so the Cu²⁺/Cu⁺ cycle was completed. Similarly, •OH radicals are the dominant reactive species during the degradation of MO.

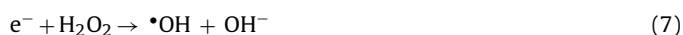
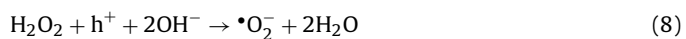


Fig. 8. UV–vis absorption spectra of an aqueous solution of MO (a) 0H₂O₂-10CuO; (b) 0.2H₂O₂-10CuO; (c) 0.5H₂O₂-10CuO; (d) 1.0H₂O₂-10CuO; (e) 0.5H₂O₂-0CuO (f) photo degradation ratio of various samples for MO at different time.



The favorable photodegradation of MO was attributed to the synergy of H₂O₂ and the well-crystalline CuO fibers. On the one hand, abundant electrons were accepted by H₂O₂ and additional

•OH were produced, which increased the oxidation capacity of the whole system. H₂O₂ is an excellent electron acceptor and the capture of charge carriers by H₂O₂ was more effective than that by O₂ and H₂O [50]. So the utilization ratio of photogenerated electrons was elevated and the recombination of electrons and holes was decreased. On the other hand, the well-crystalline CuO fibers

which is very beneficial for H_2O_2 to capture the electrons. It is well known that crystal defects always act as charge-trapping sites, where electron-hole recombination processes take place [52]. Thus, the well-crystalline of CuO fibers provide less recombination sites for carriers, resulting in a decrease in electron-hole recombination probability and in higher quantum yields during the photocatalytic reaction. While only the H_2O_2 was added in the photocatalytic process, no photocatalytic reaction was occurred for the oxidizability of H_2O_2 was insufficient to oxidize the MO. The higher photocatalytic activity when the H_2O_2 existed was proved by many photocatalysis systems [52–55].

4. Conclusions

The well-crystalline CuO fibers were successfully prepared via electrospinning and subsequent calcination. A series of parameters in the electrospinning process were adjusted and explored. Results show that the spinnability and morphology of composite fibers are closely related to these parameters. Besides, the calcination temperature played a crucial role in keeping great microstructure and obtaining excellent crystallinity for CuO fibers. In this work, the well-crystalline CuO fibers consisted of numerous CuO grains could be obtained by calcining precursor fibers at 550°C for 2 h. The as-prepared CuO fibers exhibited high photocatalytic activities for MO degradation in the presence of $238.8\text{ mmol/L H}_2\text{O}_2$ and the degradation ratio could be up to 83% in 180 min, which is 3.8 times as much as one by P25 alone under the irradiation of Xe lamp. The adding volume of H_2O_2 affected the degradation rate and 0.5 mL is suitable in the experiment. Meanwhile, the good crystallinity of CuO fibers made the electrons transferred easier, which is also favorable for increasing the photocatalytic activity. In conclusion, the combination of a highly crystalline CuO and H_2O_2 is very effective for the MO degradation. The $\cdot\text{OH}$ radicals should be the dominant active species that are responsible for the MO degradation in the presence of H_2O_2 . Finally, the mechanisms about the formation of CuO fibers and the photo Fenton-like mechanism were discussed in detail. An understanding of photo Fenton-like activities of the CuO fibers will be useful for improving the quality of the wastewater.

Fig. 9. PL spectra of CuO fibers.

Fig. 10. Trapping experiments with different quenchers.

were endowed with great electron transportation rate because electron scattering decreased and the electron transportation rate elevated caused by their ordered crystal arrangements of lattice,

Fig. 11. Schematic illustration of the photocatalytic mechanism of CuO fibers under irradiation.

Acknowledgement

This work was supported in part by the project from National Basic Research Program of China (973 Program, 2013CB632401), the program for Taishan Scholars, the projects from National Natural Science Foundation of China (51202090, 51402123), the Science and Technology Projects of Colleges and Universities of Shandong Province (J12LA06) and China Scholarship Council.

References

- [1] T. Ghodselahi, H. Zahrabi, M. Heidari Saani, M.A. Vesaghi, CO gas sensor properties of Cu@CuO core-shell nanoparticles based on localized surface plasmon resonance, *J. Phys. Chem. C* 115 (2011) 22126–22130.
- [2] H.Q. Jiang, H. Endo, H. Natori, M. Nagai, K. Kobayashi, Fabrication and efficient photocatalytic degradation of methylene blue over CuO/BiVO₄ composite under visible-light irradiation, *Mater. Res. Bull.* 44 (2009) 700–706.
- [3] Y.M. Li, J. Liang, Z.L. Tao, J. Chen, CuO particles and plates: synthesis and gas-sensor application, *Mater. Res. Bull.* 43 (2008) 2380–2385.
- [4] J. Herran, G.G. Mandayo, I. Ayerdi, E. Castano, Influence of silver as an additive on BaTiO₃-CuO thin film for CO₂ monitoring, *Sens. Actuators B: Chem.* 129 (2008) 386–390.
- [5] S.P. Meshram, P.V. Adhyapak, U.P. Mulik, D.P. Amalnerkar, Facile synthesis of CuO nanomorphs and their morphology dependent sunlight driven photocatalytic properties, *Chem. Eng. J.* 204–206 (2012) 158–168.
- [6] Z.L. Zhang, H. Chen, H.W. Che, Y.H. Wang, F.B. Su, Facile synthesis of high surface area hedgehog-like CuO microspheres with improved lithium storage properties, *Mater. Chem. Phys.* 138 (2013) 593–600.
- [7] J.R. Huang, G.J. Fu, C.C. Shi, X.Y. Wang, M.H. Zhai, C.P. Gu, Novel porous CuO microrods: synthesis, characterization, and their photocatalysis property, *J. Phys. Chem. Solids* 75 (2014) 1011–1016.
- [8] N.E. Alireza, H. Shohreh, Solar photodecolorization of methylene blue by CuO/X zeolite as a heterogeneous catalyst, *Appl. Catal. A: Gen.* 388 (2010) 149–159.
- [9] Z.L. Liu, J.C. Deng, J.J. Deng, F.F. Li, Fabrication and photocatalysis of CuO/ZnO nano-composites via a new method, *Mater. Sci. Eng. B* 150 (2008) 99–104.
- [10] C. Yang, X.D. Cao, S.J. Wang, L. Zhang, F. Xiao, X.T. Sua, J.D. Wang, Complex-directed hybridization of CuO/ZnO nanostructures and their gas sensing and photocatalytic properties, *Ceram. Int.* 41 (2015) 1749–1756.
- [11] L.L. Zhu, M.H. Hong, G. Wei Ho, Fabrication of wheat grain textured TiO₂/CuO composite nanofibers for enhanced solar H₂ generation and degradation performance, *Nano Energy* 11 (2015) 28–37.
- [12] H.L. Xia, H.S. Zhuang, T. Zhang, D.C. Xiao, Photocatalytic degradation of Acid Blue 62 over CuO-SnO₂ nanocomposite photocatalyst under simulated sunlight, *J. Environ. Sci-China* 19 (2007) 1141–1145.
- [13] W.R. Zhao, Y. Wang, Y. Yang, J. Tang, Y.N. Yang, Carbon spheres supported visible-light-driven CuO-BiVO₄ heterojunction: preparation characterization, and photocatalytic properties, *Appl. Catal. B: Environ.* 115–116 (2012) 90–99.
- [14] L.L. Cheng, Y.J. Wang, D.H. Huang, T. Nguyen, Y. Jiang, H.C. Yu, N. Ding, G.J. Ding, Z. Jiao, Facile synthesis of size-tunable CuO/graphene composites and their high photocatalytic performance, *Mater. Res. Bull.* 61 (2015) 409–414.
- [15] N.E. Alireza, Z.M. Hamidreza, Heterogeneous photodecolorization of mixture of methylene blue and bromophenol blue using CuO-nano-clinoptilolite, *J. Ind. Eng. Chem.* 20 (2014) 1421–1431.
- [16] R. Sahay, J. Sundaramurthy, P. Suresh Kumar, V. Thavasi, S.G. Mhaisalkar, S. Ramakrishna, Synthesis and characterization of CuO nanofibers, and investigation for its suitability as blocking layer in ZnO NPs based dye sensitized solar cell and as photocatalyst in organic dye degradation, *J. Solid State Chem.* 186 (2012) 261–267.
- [17] Y. Li, X.Y. Yang, J. Rooke, G.V. Tendeloo, B.L. Su, Ultralong Cu(OH)₂ and CuO nanowire bundles: PEG200-directed crystal growth for enhanced photocatalytic performance, *J. Colloid Interface Sci.* 348 (2010) 303–312.
- [18] S.P. Meshram, P.V. Adhyapak, U.P. Mulik, D.P. Amalnerkar, Facile synthesis of CuO nanomorphs and their morphology dependent sunlight driven photocatalytic properties, *Chem. Eng. J.* 204–206 (2012) 158–168.
- [19] S. Behrouz, A.G. Ebrahim, A.K. Yashar, K. Ali, Preparation of CuO nanopowders and their catalytic activity in photodegradation of Rhodamine-B, *Adv. Powder Technol.* 25 (2014) 1043–1052.
- [20] G. Nixon Samuel Vijayakumar, S. Devashankar, M. Rathnakumari, P. Sureshkumar, Synthesis of electrospun ZnO/CuO nanocomposite fibers and their dielectric and non-linear optic studies, *J. Alloys Compd.* 507 (2010) 225–229.
- [21] V.T. Le, H. Kim, A. Ghosh, J. Kim, J. Chang, Q.A. Vu, D.T. Pham, J.H. Lee, S.W. Kim, Y.H. Lee, Coaxial fiber supercapacitor using all-carbon material electrodes, *ACS Nano* 7 (2013) 5940–5947.
- [22] C.J. Dong, X.X. Xing, N. Chen, X. Liu, Y.D. Wang, Biomimetic synthesis of hollow CuO fibers for low-ppm-level n-propanol detection via a facile solution combustion method, *Sens. Actuators B* 230 (2016) 1–8.
- [23] Y.L. Zou, Y. Li, Y. Guo, Q.J. Zhou, D.M. An, Ultrasound-assisted synthesis of CuO nanostructures templated by cotton fibers, *Mater. Res. Bull.* 47 (2012) 3135–3140.
- [24] Q.Y. Liu, J. Li, Y.Q. Zhao, Y. Zhou, C.R. Li, CdS nanoparticle-functionalized natural cotton cellulose electrospun nanofibers for visible light photocatalysis, *Mater. Lett.* 138 (2015) 89–91.
- [25] S.L. Bai, W.T. Guo, J.H. Sun, J. Li, Y. Tian, A. Chen, R.X. Luo, D.Q. Li, Synthesis of SnO₂-CuO heterojunction using electrospinning and application in detecting of CO, *Sens. Actuators B* 226 (2016) 96–103.
- [26] A. Greiner, J.H. Wendorff, Electrospinning: a fascinating method for the preparation of ultrathin fibers, *Angew. Chem. Int. Ed.* 46 (2007) 5670–5703.
- [27] S. Agarwal, A. Greiner, J.H. Wendorff, Functional materials by electrospinning of polymers, *Prog. Polym. Sci.* 38 (2013) 963–991.
- [28] S.W. Choi, A. Katoch, J. Zhang, S.S. Kim, Electrospun nanofibers of CuO/SnO₂ nanocomposite as semiconductor gas sensors for H₂S detection, *Sens. Actuators B* 176 (2013) 585–591.
- [29] J. Kong, Z. Liu, Z. Yang, H.R. Tan, S. Xiong, S.Y. Wong, X. Li, X. Lu, Carbon/SnO₂/carbon core/shell/shell hybrid nanofibers: tailored nanostructure for the anode of lithium ion batteries with high reversibility and rate capacity, *Nanoscale* 4 (2012) 525–530.
- [30] C.C. Chou, C.F. Huang, M.J. Chen, Fabrication and characterization of solid oxide fuel cell anode with impregnated catalytic NiCeO₂ nano-particles on 8YSZ fibers, *Adv. Mater. Res.* 287–290 (2011) 2485–2488.
- [31] A. Vild, S. Teixeira, K. Kühn, G. Cuniberti, V. Sencadas, Orthogonal experimental design of titanium dioxide-poly(methyl methacrylate) electrospun nanocomposite membranes for photocatalytic applications, *J. Environ. Chem. Eng.* 4 (2016) 3151–3158.
- [32] F. Kayaci, S. Vempati, C. Ozgit-Akgun, N. Biyikli, T. Uyar, Enhanced photocatalytic activity of homoassembled ZnO nanostructures on electrospun polymeric nanofibers: a combination of atomic layer deposition and hydrothermal growth, *Appl. Catal. B: Environ.* 156–157 (2014) 173–183.
- [33] S.S. Lee, H.W. Bai, Z.Y. Liu, D.D. Sun, Optimization and an insightful properties-activity study of electrospun TiO₂/CuO composite nanofibers for efficient photocatalytic H₂ generation, *Appl. Catal. B: Environ.* 140–141 (2013) 68–81.
- [34] P. Bansal, A. Verma, Synergistic effect of dual process (photocatalysis and photo-Fenton) for the degradation of Cephalexin using TiO₂ immobilized novel clay beads with waste fly ash/foundry sand, *J. Photochem. Photobiol. A* 342 (2017) 131–142.
- [35] S. Guo, G.K. Zhang, Y.D. Guo, J.C. Yu, Graphene oxide-Fe₂O₃ hybrid material as highly efficient heterogeneous catalyst for degradation of organic contaminants, *Carbon* 60 (2013) 437–444.
- [36] H.J. Lee, H.S. Lee, C.H. Lee, Degradation of diclofenac and carbamazepine by the copper(II)-catalyzed dark and photo-assisted Fenton-like systems, *Chem. Eng. J.* 245 (2014) 258–264.
- [37] S.L. Wang, Q. Li, F.X. Chen, J. Ke, R. Chen, HEPES-mediated controllable synthesis of hierarchical CuO nanostructures and their analogous photo-Fenton and antibacterial performance, *Adv. Powder Technol.* 28 (2017) 1332–1339.
- [38] H. Siddiqui, M.S. Qureshi, F.Z. Haque, One-step, template-free hydrothermal synthesis of Cu tetrapods, *Optik* 125 (2014) 4663–4667.
- [39] Y.Q. Wang, T.T. Jiang, D.W. Meng, H.Y. Jin, M.H. Yu, Controllable fabrication of nanowire-like CuO film by anodization and its properties, *Appl. Surf. Sci.* 349 (2015) 636–643.
- [40] H. Siddiqui, M.S. Qureshi, F.Z. Haque, Valuation of copper oxide (CuO) nanoflakes for its suitability as an absorbing material in solar cells fabrication, *Optik* 127 (2016) 3713–3717.
- [41] P. Chand, A. Gaur, A. Kumar, Structural, optical and ferroelectric behavior of CuO nanostructures synthesized at different pH values, *Superlattices Microstruct.* 60 (2013) 129–138.
- [42] M. Sabbaghian, A.S. Shahvelayati, K. Madankar, CuO nanostructures: optical properties and morphology control by pyridinium-based ionic liquids, *Spectrochim. Acta Part A* 135 (2015) 662–668.
- [43] A.S. Lanje, S.J. Shrama, R.B. Pote, Synthesis and optical characterization of copper oxide nanoparticles, *Arch. Phys. Res.* 1 (2010) 36–49.
- [44] J.S.K. Arockiasamy, J. Irudayaraj, Natural dye sensitized CuO nanorods for luminescence applications, *Ceram. Int.* 42 (2016) 6198–6205.
- [45] W.R. Zhao, Y. Wang, Y. Yang, J. Tang, Y.N. Yang, Carbon spheres supported visible-light-driven CuO-BiVO₄ heterojunction: preparation characterization, and photocatalytic properties, *Appl. Catal. B: Environ.* 115–116 (2012) 90–99.
- [46] D.D. Tang, G.K. Zhang, Fabrication of AgFeO₂/g-C₃N₄ nanocatalyst with enhanced and stable photocatalytic performance, *Appl. Surf. Sci.* 391 (2017) 415–422.
- [47] Z. Wan, G.K. Zhang, X.Y. Wu, S. Yin, Novel visible-light-driven Z-scheme Bi₁₂GeO₂₀/g-C₃N₄ photocatalyst: oxygen-induced pathway of organic pollutants degradation and proton assisted electron transfer mechanism of Cr(VI) reduction, *Appl. Catal. B: Environ.* 207 (2017) 17–26.
- [48] A. Nezamzadeh-Ejhi, S. Hushmandrad, Solar photodecolorization of methylene blue by CuO/X zeolite as a heterogeneous catalyst, *Appl. Catal. A: Gen.* 388 (2010) 149–159.
- [49] M. Paschoalino, N.C. Guedes, W. Jardim, E. Mielczarskib, J.A. Mielczarskib, P. Bowenc, J. Kiwid, Inactivation of E. coli mediated by high surface area CuO accelerated by light irradiation >360 nm, *J. Photochem. Photobiol.* 199 (2008) 105–111.
- [50] L. Korösi, M. Prato, A. Scarpellini, J. Kovács, D. Dömötör, T. Kovács, S. Papp, H₂O₂-assisted photocatalysis on flower-like rutile TiO₂ nanostructures: rapid dye degradation and inactivation of bacteria, *Appl. Surf. Sci.* 365 (2016) 171–179.

- [51] S. Guo, G.K. Zhang, J.Q. Wang, Photo-Fenton degradation of rhodamine B using Fe_2O_3 -Kaolin as heterogeneous catalyst: characterization, process optimization and mechanism, *J. Colloid Interface Sci.* 433 (2014) 1–8.
- [52] L. Kőrösi, M. Prato, A. Scarpellini, J. Kovács, D. Dömötör, Tamás Kovács, Szilvia Papp, H_2O_2 -assisted photocatalysis on flower-like rutile TiO_2 nanostructures: rapid dye degradation and inactivation of bacteria, *Appl. Surf. Sci.* 365 (2016) 171–179.
- [53] Y.Y. Huang, F.Q. Sun, T.X. Wu, Q.S. Wu, Z. Huang, H. Su, Z.H. Zhang, Photochemical preparation of CdS hollow microspheres at room temperature and their use in visible-light photocatalysis, *J. Solid State Chem.* 184 (2011) 644–648.
- [54] K. Rekab, C. Lepeytre, M. Dunand, F. Dappozze, J.M. Herrmann, C. Guillard, H_2O_2 and/or photocatalysis under UV-C irradiation for the removal of EDTA, a chelating agent present in nuclear waste waters, *Appl. Catal., A: Gen.* 488 (2014) 103–110.
- [55] M. Jiménez-Tototzintle, I. Oller, A. Hernández-Ramírez, S. Malato, M.I. Maldonado, Remediation of agro-food industry effluents by biotreatment combined with supported $\text{TiO}_2/\text{H}_2\text{O}_2$ solar photocatalysis, *Chem. Eng. J.* 273 (2015) 205–213.